Reactions of Laser-Ablated Osmium and Ruthenium Atoms with Nitric Oxide in Neon and Argon. Matrix Infrared Spectra and Density Functional Calculations of $Os(NO)_{1-3}$, $Ru(NO)_{1-3}$, NOsO, NRuO, $OsNO^+$ and $RuNO^+$

Angelo Citra and Lester Andrews*

Department of Chemistry, University of Virginia, Charlottesville, Virginia 22904-4319

Received: May 8, 2000; In Final Form: July 19, 2000

Laser-ablated osmium and ruthenium are reacted with nitric oxide and the products are isolated in solid neon and argon. The primary products in both neon and argon are the nitrosyl complexes $M(NO)_{1-3}$. Sharp, weak bands due to the mononitrosyl cations are also observed. The insertion products NMO observed for both metals differ in their stability relative to MNO; NOsO is more stable than OsNO whereas the reverse is the case for RuNO and NRuO. Density functional theory (DFT) calculations effectively reproduce the experimental observations and predict frequencies of chemically useful accuracy. The calculated isotopic ratios are also in very good agreement with experiment, showing that DFT correctly describes the normal modes in these molecules.

Introduction

Nitrosyls of the Group 8 metals are of interest due to the existence of long-lived metastable states produced by light irradiation of the material at sufficiently low temperatures.[1−6] Such materials could form the basis of storage devices because the crystals in the excited states exhibit different absorption properties from the ground state. An X-ray diffraction study of two metastable states of $Na_2[Fe(CN)_5NO]\cdot 2H_2O$ show that the nature of the binding of NO to the metal center is very different from that in the ground state.[1] In one the nitrosyl group is bound to iron by the oxygen atom, and in the other the NO group is bound in a side-on configuration. Such metastable configurations can be studied for the isolated MNO subunit via matrix isolation spectroscopy, where an inert matrix maintained at cryogenic temperatures can kinetically stabilize higher energy structures that would otherwise rapidly rearrange to a more stable form. The side-bound species Fe[NO] was observed previously in this laboratory, in addition to the more stable mononitrosyl FeNO and possibly the insertion product NFeO.[7]

In this work, reactions between the second- and third-row metals in the iron group, ruthenium and osmium, and nitric oxide are studied by matrix isolation spectroscopy. Analogous vertical investigations for the Group 4, 5, 6, 7, and 11 metals reveal similar products within a given group.[8−16] The mononitrosyl and insertion products are identified, as is the side-bound Os-[NO] molecule. The mononitrosyls exhibit a marked sensitivity to UV/visible light, consistent with the larger nitrosyl complexes of these metals. The higher complexes $M(NO)_2$ and $M(NO)_3$ are also observed and show the same frequency ordering as was found for the iron nitrosyls.[7] Finally, the cationic species $OsNO^+$ and $RuNO^+$ are observed, but the corresponding anions could not be identified. The results complement a previous study of the relationship between the physical properties and charge in a series of ruthenium complexes.[17]

Experimental Section

The experiment for laser ablation and matrix isolation has been described in detail previously.[18,19] Briefly, the Nd:YAG laser fundamental (1064 nm, 10 Hz repetition rate with 10 ns pulse width) was focused on rotating ruthenium and osmium targets (Johnson−Matthey, E-Vac). Laser energies ranging from 5 to 50 mJ/pulse were used. In experiments with neon, a 10% neutral density filter was used to reduce the laser energy. Laser-ablated metal atoms, cations, and electrons were co-deposited with nitric oxide at 0.1−0.3% in argon or 0.1−0.02% in neon onto a 7−8 K or 4−5 K CsI window at 2−4 mmol/h for 30 min to 2 h. Several isotopic samples ($^{14}N^{16}O$, Matheson; $^{15}N^{16}O$, MDS isotopes, 99%; $^{15}N^{18}O$, Isotec, 99%) and selected mixtures were used. Infrared spectra were recorded at 0.5 cm^{-1} resolution on a Nicolet 750 spectrometer with 0.1 cm^{-1} accuracy using a HgCdTe detector. Matrix samples were annealed at a range of temperatures (20−45 K, argon, and 6−12 K, neon) and subjected to broadband photolysis by a medium-pressure mercury arc (Philips, 175 W) with the globe removed ($\lambda > 240$ nm).

Calculations

Density functional theory (DFT) calculations were performed on the ruthenium and osmium nitrosyls using the Gaussian 94 program.[20] The BPW91 functional was used in all calculations, and the B3LYP functional was employed for comparison in selected cases.[21−23] The 6-311+G(d) basis set was used to represent nitrogen and oxygen,[24] and the LanL2DZ ECP basis set was used for osmium and ruthenium.[25,26]

Results

Absorptions observed for osmium and ruthenium nitrosyl products in pure and mixed isotopic experiments in solid neon and argon are listed in Tables 1−4. Figures 1−7 show spectra in neon and argon matricies in both nitrosyl and nitride-oxide regions. Additional bands due to NO, $(NO)_2$, N_2O_3, $(NO)_2^+$, $(NO)_2^-$, NO_2, and NO_2^- common to experiments with laser-ablated metal and nitric oxide are not listed in the tables.[7] The optimized geometries and associated harmonic frequencies of product molecules calculated using DFT are summarized in

10.1021/jp001700t CCC: $19.00
Published on Web 08/25/2000

TABLE 1: Infrared Absorptions (cm^{-1}) from Co-deposition of Laser-Ablated Osmium Atoms with NO in Excess Neon at 4 K

$^{14}N^{16}O$	$^{15}N^{16}O$ [$^{14}N^{16}O/^{15}N^{16}O$]	$^{15}N^{18}O$ [$^{15}N^{16}O/^{15}N^{18}O$]	$^{14}N^{16}O + ^{15}N^{16}O$	assignment
1921.8	1882.4 [1.0209]	1842.0 [1.0219]	1921.8, 1882.4	$OsNO^+$
1919.6	1879.8 [1.0212]	1839.7 [1.0218]	1919.6, 1879.8	$OsNO^+$ (site)
1834.7	1797.8 [1.0205]	*b*	*b*	$Os(NO)_2$
1818.1	1782.9 [1.0197]	*b*	1818.1, 1797.3, 1782.9	?
1813.7	1772.1 [1.0235]	1738.3 [1.0194]	1813.7, 1772.1	?
1809.4	1769.5 [1.0225]	1735.9 [1.0209]	1809.4, 1769.5	OsNO
1797.3	1756.1 [1.0235]	1722.8 [1.0193]	*b*	?
1756.6	1720.1 [1.0212]	*a*	*b*	$[Os(NO)_3]$
1753.2	1717.0 [1.0211]	*a*	*b*	$[Os(NO)_3]$
1734.1	1699.2 [1.0205]	*a*	1734.1, 1714.5, 1699.2	$Os(NO)_2$ (site)
1733.2	1697.9 [1.0208]	*a*	1733.2, 1713.2, 1697.9	$Os(NO)_2$ (site)
1731.9	1696.6 [1.0208]	1658.4 [1.0230]	1731.9, 1708.3, 1696.6	$Os(NO)_2$ (site)
1730.1	1695.1 [1.0206]	*a*	1730.1, 1706.9, 1695.1	$Os(NO)_2$ (site)
1726.9	1691.7 [1.0208]	1654.1 [1.0227]	1726.9, 1705.0, 1691.7	$Os(NO)_2$
1725.5	1693.1 [1.0191]	1652.2 [1.0248]	1725.5, 1704.0, 1693.1	$Os(NO)_2$ (site)
1708.3	1668.9 [1.0236]	1630.6 [1.0235]	b	?
1168.0	1148.8 [1.0167]	1117.5 [1.0280]	1168.0, 1148.8	Os[NO]
1135.9	1100.4 [1.0323]	1100.4	1135.9, 1100.4	OsN
1057.6	1026.3 [1.0305]	1023.3 [1.0029]	1057.6, 1026.3	NOsO
1055.7	1024.3 [1.0307]	1021.9 [1.0023]	1055.7, 1024.3	NOsO (site)
892.0	890.5 [1.0017]	846.7 [1.0517]	892.0, 890.5	NOsO
857.2	856.5 [1.0010]	814.0 [1.0522]	857.0	NOsO−NO
855.5	854.9 [1.0010]	*a*	855.1	NOsO−NO (site)

[a] Band not observed in this experiment. [b] Spectral region too congested to observe bands.

TABLE 2: Infrared Absorptions (cm^{-1}) from Co-deposition of Laser-Ablated Osmium Atoms with NO in Excess Argon at 8 K

^{14}N-^{16}O	^{15}N-^{16}O [$^{14}N^{16}O/^{15}N^{16}O$]	^{15}N-^{18}O [$^{15}N^{16}O/^{15}N^{18}O$]	^{14}N-$^{16}O + ^{15}N$-^{16}O	assignment
1901.5	1862.3 [1.0210]	1823.3 [1.0214]	1901.5, b	$OsNO^+$
1897.4	*a*	*a*	1897.4, b	$OsNO^+$ site
1823.8	*b*	*b*	*b*	$Os(NO)_2$
1815.8	*b*	*b*	*b*	$Os(NO)_2$
1811.1	*b*	*b*	*b*	$Os(NO)_2$
1789.1	1749.9 [1.0224]	1716.6 [1.0194]	1789.1, 1749.9	OsNO
1763.1	1726.5 [1.0218]	*a*	*b*	$Os_x(NO)_y$
1748.8	1713.6 [1.0205]	1675.3 [1.0229]	*b*	$Os(NO)_3$ (site)
1745.5	1710.9 [1.0202]	1671.8 [1.0234]	*b*	$Os(NO)_3$
1723.2	1687.7 [1.0210]	1651.4 [1.0220]	1723.2, 1702.8, 1687.7	$Os(NO)_2$
1717.9	1683.9 [1.0202]	1644.6 [1.0239]	1717.9, 1697.6, 1683.9	$Os(NO)_2$
1712.5	1678.5 [1.0203]	1639.6 [1.0237]	1712.5, 1692.5, 1678.5	$Os(NO)_2$
1154.5	1133.9 [1.0182]	1105.4 [1.0258]	*a*	?
1149.5	1128.8 [1.0183]	1101.0 [1.0253]	*a*	?
1132.6	1114.2 [1.0165]	1083.5 [1.0283]	1132.6, 1114.2	Os[NO]
1052.0	1021.3 [1.0301]	1017.7 [1.0035]	1052.0, 1021.3	NOsO
886.9	885.3 [1.0018]	841.9 [1.0516]	886.9, 885.3	NOsO

[a] Band not observed in this experiment. [b] Spectral region too congested to observe bands.

Tables 5−8, reaction energies are in Table 9, and additional force constant information is included in Tables 10−11 and Figure 8.

Discussion

New product molecules are identified by isotopic substitution and DFT isotopic frequency calculations as follows.

$Os(NO)_{1-3}$. The primary reaction products in both neon and argon experiments are OsNO and $Os(NO)_2$. In neon experiments with $^{14}N^{16}O$, annealing cycles produce a strong 1809.4 cm^{-1} band followed by a 1726.9 cm^{-1} absorption, which also grows in strongly during annealing, as shown in Figure 1 for a dilute sample of 0.04% NO in neon. These bands shift to 1769.5 and 1691.7 cm^{-1} with $^{15}N^{16}O$ and to 1735.9 and 1654.1 cm^{-1} with $^{15}N^{18}O$, which are appropriate for N−O vibrations. The origins of these bands are clearly revealed by the low concentration $^{14}N^{16}O + ^{15}N^{16}O$ neon matrix experiment shown in Figure 2b−f where the 1809.4 and 1726.9 cm^{-1} bands exhibit doublet and triplet mixed isotopic mulitplets, characteristic of mono and dinitrosyl complexes. The argon matrix counterparts for these bands are slightly red shifted relative to neon, which is typical for matrix-isolated species.[27]

The DFT calculations for these species reproduce the experimental results very well; the BPW91 frequency for OsNO is only slightly higher than experiment, and the B3LYP frequency requires a scale factor of 0.967, which is typical for this functional.[28] Both functionals predict a $^2\Delta$ ground state, with other doublet and quartet states lying considerably higher in energy. It should be noted that this molecule has uncommonly high $^{14}N^{16}O/^{15}N^{16}O$ and low $^{15}N^{16}O/^{15}N^{18}O$ isotopic ratios of 1.0224 and 1.0194, compared to more typical values of ∼1.020 and ∼1.025 observed in other metal mononitrosyls.[7−16] This is due to the unusually large coupling between the Os−N and N−O stretching modes that increases the participation of the nitrogen atom in the latter mode. This strong coupling is due in part to the linear geometry, which maximizes the mechanical coupling through the central atom, and also to the high strength of the Os−N bond. This is apparent from the DFT calculations,

TABLE 3: Infrared Absorptions (cm^{-1}) from Co-deposition of Laser-Ablated Ruthenium Atoms with NO in Excess Neon at 4 K

$^{14}N^{16}O$	$^{15}N^{16}O$ [$^{14}N^{16}O/^{15}N^{16}O$]	$^{15}N^{18}O$ [$^{15}N^{16}O/^{15}N^{18}O$]	$^{14}N^{16}O + {}^{15}N^{16}O$	assignment
1918.0	1879.7 [1.0205]	1835.6 [1.0240]	1918.0, 1879.7	$RuNO^+$
1915.2	*b*	*a*	1915.2	$RuNO^+$ (site)
1805.3	1768.6 [1.0208]	1730.0 [1.0224]	*a*, *b*	$Ru(NO)_2$
1790.8	*b*	1712.3	*b*	RuNO (site)
1785.8	*b*	1712.3	*b*	RuNO
1753.1	1719.0 [1.0198]	1678.2 [1.0243]	*b*	$Ru(NO)_3$ (site)
1742.3	1709.0 [1.0195]	1666.8 [1.0253]	*b*	$Ru(NO)_3$ (site)
1741.1	1707.7 [1.0196]	1666.5 [1.0247]	*b*	$Ru(NO)_3$
1730.2	1697.4 [1.0193]	1656.1 [1.0249]	*a*	$Ru(NO)_2$ (site)
1728.3	1695.6 [1.0193]	1654.4 [1.0249]	*a*	$Ru(NO)_2$ (site)
1726.2	1693.0 [1.0196]	1652.4 [1.0246]	*a*	$Ru(NO)_2$ (site)
1721.4	1687.5 [1.0201]	1648.6 [1.0236]	1721.4, 1700.2, 1687.5	$Ru(NO)_2$
1719.1	1684.9 [1.0203]	1646.5 [1.0233]	1719.1, 1697.5, 1684.9	$Ru(NO)_2$ (site)
1661.4	1632.9 [1.0175]	1587.8 [1.0284]	1661.4, 1632.9	?
991.5	963.5 [1.0291]	960.6 [1.0030]	991.5, 963.5	NRuO
800.4	799.7 [1.0009]	762.9 [1.0482]	800.4, 799.7	NRuO

[a] The band was not observed in this experiment. [b] Same as Tables 1, 2, and 4.

TABLE 4: Infrared Absorptions (cm^{-1}) from Co-deposition of Laser-Ablated Ruthenium Atoms with NO in Excess Argon at 7 K

$^{14}N^{16}O$	$^{15}N^{16}O$ [$^{14}N^{16}O/^{15}N^{16}O$]	$^{15}N^{18}O$ [$^{15}N^{16}O/^{15}N^{18}O$]	$^{14}N^{16}O + {}^{15}N^{16}O$	assignment
1848.4	1820.7 [1.0152]	*a*	*b*	?
1846.0	*a*	*a*	*b*	?
1773.0	1736.0 [1.0213]	*b*	1773.0, 1736.0	RuNO (site)
1770.7	1733.8 [1.0213]	*b*	1770.7, 1733.8	RuNO (site)
1765.9	1729.2 [1.0212]	1693.0 [1.0214]	1765.9, 1729.2	RuNO
1743.8	1710.3 [1.0196]	1669.4 [1.0245]	*b*	$Ru(NO)_3$ (site)
1738.9	1705.4 [1.0196]	1664.9 [1.0243]	*b*	$Ru(NO)_3$
1731.6	1697.2 [1.0203]	1658.7 [1.0232]	*b*	$Ru(NO)_3$ (site)
1715.2	1682.6 [1.0194]	1642.0 [1.0247]	*b*	$Ru(NO)_2$ (site)
1713.8	1681.5 [1.0192]	1640.3 [1.0251]	*b*	$Ru(NO)_2$ (site)
1711.6	1679.6 [1.0191]	1639.7 [1.0243]	*b*	$Ru(NO)_2$ (site)
1709.6	1677.5 [1.0191]	*b*	1709.6, 1690.1, 1677.5	$Ru(NO)_2$
1707.7	1675.7 [1.0191]	1635.9 [1.0243]	*b*	$Ru(NO)_2$ (site)
1692.8	1660.5 [1.0195]	1617.4 [1.0266]	*b*	$Ru_x(NO)_y$
1688.0	1657.3 [1.0185]	1614.2 [1.0267]	*b*	$Ru_x(NO)_y$
1671.4	1640.6 [1.0188]	1598.8 [1.0261]	*b*	$Ru_x(NO)_y$
1650.4	1621.8 [1.0176]	1578.3 [1.0276]	*b*	$Ru_x(NO)_y$
1614.1	1587.3 [1.0169]	*a*	1614.1, 1603.1, 1594.7, 1587.0	?
991.8	962.6 [1.0303]	960.5 [1.0022]	991.8, 962.6	NRuO
803.0	802.2 [1.0010]	765.2 [1.0484]	*c*	NRuO

[a] Band not observed in this experiment. [b] Spectral region too congested to observe bands. [c] Unresolved bands.

which predict an Os−N frequency of 696.1 cm^{-1} (BPW91), compared to, for example, the equivalent mode in PtNO calculated at 610.6 cm^{-1}.[16] The strength of this bond is not surprising considering the derived force constants in NOsN,[29] NOsO (this study), and various osmium nitrido complexes.[30] As expected from this discussion, the DFT calculations show that the nitrogen motion has the greatest amplitude in the nitrosyl stretching mode, moving in the opposite direction to the metal and oxygen atoms, and predict isotopic ratios of 1.0231 and 1.0194, which are in excellent agreement with the experimental values.

Good agreement between experiment and theory is also found for $Os(NO)_2$, where both density functionals predict a nonlinear singlet ground state. The out-of-phase nitrosyl stretching frequency of 1751.7 cm^{-1} calculated using BPW91 is only 24.8 cm^{-1} higher than the experimental value in neon, and the B3LYP value of 1793.0 cm^{-1} requires a scale factor of 0.958, a typical result for metal nitrosyls.[7−16] The $^{14}N^{16}O/^{15}N^{16}O$ and $^{15}N^{16}O/^{15}N^{18}O$ isotopic ratios calculated for the out-of-phase nitrosyl stretching mode using BPW91 are 1.0210 and 1.0230, in excellent agreement with the experiment values of 1.0208 and 1.0227 (neon). The BPW91 calculation predicts the in-phase nitrosyl stretching frequency to be 1817.6 cm^{-1}, with only a quarter of the intensity of the in-phase mode. A broad band is observed at 1834.7 cm^{-1} with approximately this relative intensity that tracks with the equally broad 1726.9 cm^{-1} band and associated matrix sites under all conditions, and is therefore assigned to the in-phase nitrosyl stretching mode of $Os(NO)_2$. The $^{15}N^{16}O$ counterpart to this band is observed at 1797.8 cm^{-1}, giving a $^{14}N^{16}O/^{15}N^{16}O$ ratio of 1.0205, in reasonable agreement with the DFT calculated value of 1.0219 for this quantity. However, the $^{15}N^{18}O$ counterpart cannot be identified.

Three prominent matrix sites are observed for $Os(NO)_2$ in argon, at 1723.2, 1717, and 1712.5 cm^{-1} (Figure 3), slightly below the neon value of 1726.9 cm^{-1}. Weaker bands at 1823.8, 1815.8, and 1811.1 cm^{-1} are appropriate for assignment to the in phase stretching mode, though the isotopic counterpart bands are somewhat ambiguous.

A sharp set of bands also grows in at 1756.6 and 1753.2 cm^{-1} at higher annealing temperatures (Figure 1). However, these and any isotopic counterparts are obscured by $(NO)_2$ absorptions in the low concentration $^{14}N^{16}O + {}^{15}N^{16}O$ neon matrix experiment (Figure 2). In argon, an analogous band at 1745.5 cm^{-1} (Figure 3) increases significantly during annealing, between the OsNO

TABLE 5: Geometries, Energies, and Frequencies Calculated for Neutral and Ionic Osmium Nitrosyls Using DFT (BPW91/LanL2DZ/6-311+G(d))

molecule	state (point group)	relative energies (kJ/mol)	$<S^2>$	geometry (Å, deg)	frequencies (cm^{-1}) [intensities (km/mol)]
OsNO	$^2\Delta$ ($C_{\infty v}$)	+82	0.7502	OsN: 1.692 NO: 1.181 ∠OsNO: 180.0	1841.6 [588], 696.1 [1], 407.0 [8]×2
	$^2\Sigma^+$ ($C_{\infty v}$)	+196	0.7500	OsN: 1.696 NO: 1.189 ∠OsNO: 180.0	/
	$^4A''$ (C_s)	+146	3.7502	OsN: 1.799 NO: 1.189 ∠OsNO: 146.7	/
Os[NO]	$^2A'$ (C_s)	+256	0.7512	OsN: 1.831 OsO: 2.071 NO: 1.284	1202.8 [146], 724.4 [34], 417.4 [5]
	$^4A'$ (C_s)	+330	3.7500	OsN: 1.921 OsO: 1.915 NO: 1.384	994.5 [25], 623.6 [15], 491.1 [1]
OsON	$^2\Delta$ ($C_{\infty v}$)	+349	0.7779	OsO: 1.776 ON: 1.189 ∠OsON: 180.0	1656.9 [304], 569.0 [0], 330.2 [4]x2
	$^2\Sigma^+$	+465	0.7565	OsO: 1.774 ON: 1.195 ∠OsON: 180.0	1632.2 [271], 580.7 [1], 308.0 [3]x2
	$^4A''$	+347	3.8236	OsO: 1.967 ON: 1.188 ∠OsON: 153.4	1570.0 [374], 373.1 [2], 222.5 [18]
NOsO	$^2A''$ (C_s)	0	0.7502	OsN: 1.668 OsO: 1.737 NOsO: 109.9	1110.1 [14], 898.6 [76], 360.0 [0]
	$^2A'$ (C_s)	+72	0.7501	OsN: 1.679 OsO: 1.761 NOsO: 119.3	1069.6 [30], 868.8 [102], 313.3 [2]
	$^4A''$ (C_s)	+57	3.7500	OsN: 1.685 OsO: 1.767 NOsO: 124.8	1060.8 [31], 854.2 [90], 293.6 [1]
$OsNO^+$	$^1\Sigma^+$ ($C_{\infty v}$)	+157	/	OsN: 1.725 NO: 1.158 ∠pOsNO: 180.0	/
	$^1\Delta$ ($C_{\infty v}$)	+71	0.0361	OsN: 1.728 NO: 1.152 ∠OsNO: 180.0	1955.6 [439], 659.5 [5], 405.0 [7]x2
	$^3\Sigma^-$ ($C_{\infty v}$)	+7	2.0009	OsN: 1.732 NO: 1.146 ∠OsNO: 180.0	1990.8 [442], 652.7 [5], 402.8 [9]x2
	$^3\Delta$ ($C_{\infty v}$)	0	2.0003	OsN: 1.730 NO: 1.152 ∠OsNO: 180.0	1956.6 [431], 655.7 [4], 410.2 [7]x2
$Os(NO)_2$	$^1A_1$ (C_{2v})	0	/	OsN: 1.762 NO: 1.182 ∠OsNO: 160.0 ∠NOsN: 119.2	1817.6 [319], 1751.7 [1271], 712.0 [3], 618.7 [2], 591.0 [1], 477.0 [5], ···99.0 [1]
	$^3B_1$ (C_{2v})	+105	2.0000	OsN: 1.804 NO: 1.185 ∠OsNO: 168.3 ∠NOsN: 137.6	/
NOsO−NO	$^1A'$ (C_s)	+64	/	OsO_t: 1.746 OsN_t: 1.694 OsN: 1.882 NO: 1.163 N_tOsO_t: 117. 1 N_tOsN: 102.9 O_tOsN: 140.0 OsNO: 178.8 $\phi(ONOsO_t)$: 180.0	1842,5 [746], 1044,8 [17], 917.7 [136], 509.0 (1), 479.5 (6), ···106.1 [2]
	^3A (C_1)	+68	2.0001	OsO_t: 1.753 OsN_t: 1.697 OsN: 1.868 NO: 1.182 N_tOsO_t: 114.2 N_tOsN: 107.1 OrOsN: 129.0 OsNO: 165.8 $\phi(ONOsO_t)$: 22.8	1763.9 [530], 1014.6 [16], 887.1 [100], 508.0 [1], 453.8 [2], ···87.6 [1]

TABLE 5 (Continued)

molecule	state (point group)	relative energies (kJ/mol)	$<S^2>$	geometry (Å, deg)	frequencies (cm^{-1})
$Os(NO)_3$	$''^2A_1''$ (C_{3v})	0	0.7501	OsN: 1.821 NO: 1.177 ∠NOsN: 118.6 ∠OsNO: 173.3	1824.7 [27], 1757.2 [1367]x2, 567.4 [1], 558.1 [36]×2, 511.8 [58]x2, 512.3 [5], ···58.6 [0]
	$''^4A_2''$ (D_{3h})	+177	3.7501	OsN: 1.845 NO: 1.185 ∠NOsN: 120.0 ∠OsNO: 180.0	/

TABLE 6: Geometries, Energies, and Frequencies Calculated for Selected Neutral and Ionic Osmium Nitrosyls Using DFT (B3LYP/LanL2DZ/6-311+G(d))

molecule (ground state) [relative energy, kJ/mol]	$<S^2>$	geometry (Å, deg)	frequencies (cm^{-1}) [intensities (km/mol)]	ν(NO) scale factors	
				argon	neon
OsNO ($^2\Sigma^+$) [+173]	0.7500	OsN: 1.691 NO: 1.180 ∠OsNO: 180.0	/	/	/
OsNO ($^2\Delta$) [+55]	0.7512	OsN: 1.688 NO: 1.1711 ∠OsNO: 180.0	1870.6 [797], 703.8 [0], 416.2 [8]×2	0.956	0.967
NOsO (^{2}A") [0]	0.7505	OsN: 1.655 OsO: 1.731 NOsO: 110.0	1148.9 [17], 911.0 [89], 360.4 [1]	0.916 0.974	0.921 0.979
NOsO ($^2A'$) [+67]	0.7501	OsN: 1.667 OsO: 1.754 NOsO: 120.2	1104.7 [30], 888.8 [129], 313.0 [3]	0.952 0.998	0.957 0.996
Os[NO] ($^2A'$) [+223]	0.8081	OsN: 1.837 OsO: 2.084 NO: 1.262	1268.1 [284], 690.5 [23], 328.6 [7]	0.910	0.921
Os[NO] ($^4A'$) [+279]	3.7502	OsN: 1.946 OsO: 1.927 NO: 1.337	1106.4 [51], 627.8 [18], 486.5 [0]	/	/
OsON ($^2\Sigma^+$) [+450]	1.1747	OsO: 1.803 NO: 1.201 ∠OsON: 180.0	1529.4 [27], 511.4 [7], 235.4 [3]×2	/	/
OsON ($^2\Delta$) [+302]	1.5040	OsO: 1.809 NO: 1.202 ∠OsON: 180.0	1520.6 [247], 516.6 [6], 204.1 [2]	/	/
$OsNO^+$ ($^1\Sigma^+$) [+155]	/	OsN: 1.725 NO: 1.144 ∠OsNO: 180.0	/	/	/
$OsNO^+$ ($^1\Delta$) [+68]	0.0968	OsN: 1.730 NO: 1.138 ∠OsNO: 180.0	2014.6 [629], 660.7 [7], 413.1 [7]×2	0.944	0.954
$OsNO^+$ ($^3\Sigma^-$) [0]	2.0039	OsN: 1.736 NO: 1.133 ∠OsNO: 180.0	2047.5 [614], 643.3 [6], 407.5 [8]×2	0.929	0.939
$OsNO^+$ ($^3\Delta$) [+4]	2.0013	OsN: 1.735 NO: 1.139 ∠OsNO: 180.0	2011.5 [607], 647.8 [6], 411.8 [7]×2	0.945	0.955
$Os(NO)_2$ ($^1A_1$)	/	OsN: 1.754 NO: 1.120 ∠NOsN: 117.8 ∠OsNO: 160.1 ϕ(ONOsN): 0.0	1871.6 [444], 1793.0 [1685], 737.4 [3], 636.8 [4], 611.3 [1], ···102.3 [2]	0.958	0.963
$Os(NO)_3$ "$^2A'''$ (C_{3v})	0.7560	OsN: 1.821 NO: 1.163 ∠OsNO: 173.3	1897.7 [0], 1812.8 [1777]×2, 558.3 [0], 550.4 [69], 495.7 [90], ···23.7 [0]	0.963	[1.004]

and $Os(NO)_2$ absorptions. The $^{15}N^{16}O$ and $^{15}N^{18}O$ counterpart bands are observed, but the mixed isotopic spectra are too congested for these or any intermediate bands to be discerned. In the previous iron nitrosyl study, the most intense $Fe(NO)_3$ absorption was observed at 1742.6 cm^{-1} between the FeNO and $Fe(NO)_2$ absorptions at 1748.9 and 1731.6 cm^{-1}, so the 1745.5 cm^{-1} band is most probably due to $Os(NO)_3$. Both BPW91 and B3LYP functionals predict a doublet ground state for $Os(NO)_3$, the lowest quartet state is much higher in energy. The degenerate nitrosyl stretching mode is calculated at 1757.2 cm^{-1} with the BPW91 functional, in good agreement with the observed band, and the B3LYP value of 1812.8 cm^{-1} requires a scale factor similar to those for Os(NO) and $Os(NO)_2$. The $^{14}N^{16}O/^{15}N^{16}O$ and $^{15}N^{16}O/^{15}N^{18}O$ isotopic ratios of 1.0205 and 1.0239 calculated for the degenerate mode of $Os(NO)_3$ using the BPW91 functional are in very good agreement with the experimental values of 1.0202 and 1.0234, giving more support to the assignment of the 1745.5 cm^{-1} band in argon to $Os(NO)_3$. The optimized structure for the trinitrosyl is very close to C_{3v} but is distorted to C_s symmetry. A similar distortion is found for $Ru(NO)_3$ described below, and this is an artifact of the calculation commonly found for highly symmetric mol-

TABLE 7: Geometries, Energies, and Frequencies Calculated for Neutral and Ionic Ruthenium Nitrosyls Using DFT (BPW91/LanL2DZ/6-311+G(d))

molecule	state (point group)	relative energies (kJ/mol)[a]	<S²>	geometry (Å, deg)	grequencies (cm^{-1}) [intensities (km/mol)]
RuNO	$^2\Sigma^+$ ($C_{\infty v}$)	+42	0.7500	RuN: 1.711 NO: 1.185 ∠RuNO: 180.0	1769.8 [500], 625.2 [4], 263.3 [19]×2
	$^2\Delta$ ($C_{\infty v}$)	0	0.7504	RuN: 1.726 NO: 1.177 ∠RuNO: 180.0	1804.3 [554], 613.1 [4], 206.1 [31]×2
	$^4A''$ (C_s)	+58	3.7502	RuN: 1.827 NO: 1.191 ∠RuNO: 142.1	1657.0 [890], 587.3 [18], 300.3 [9]
NRuO	$^2A'$ (C_s)	+65	0.7500	RuN: 1.656 RuO: 1.766 NRuO: 123.3	1023.5 [57], 822.0 [117], 278.5 [4]
	$^2A''$ (C_s)	+53	0.7509	RuN: 1.653 RuO: 1.771 NRuO: 117.5	1034.3 [35], 790.2 [99], 263.7 [1]
	$^4A''$ (C_s	+96	3.7500	RuN: 1.669 RuO: 1.772 NRuO: 119.7	993.1 [47], 779.7 [60], 301.2 [5]
$RuNO^+$	$^1\Sigma^+$ ($C_{\infty v}$)	+110	/	RuN: 1.714 NO: 1.151 ∠RuNO: 180.0	/
	$^1\Delta$ ($C_{\infty v}$)	+58	0.0598	RuN: 1.774 NO: 1.144 RuNO: 180.0	1947.3 [457], 560.4 [7], 236.1 [10]
	$^3\Delta$ ($C_{\infty v}$)	0	2.0006	RuN: 1.780 NO: 1.144 RuNO: 180.0	1955.0 [446], 551.0 [5], 269.0 [9]
$Ru(NO)_2$	$^1A_1$ (C_{2v})	0	/	RuN: 1.774 NO: 1.178 ∠RuNO: 155.2 ∠NRuN: 109.7 ϕ(ONRuN): 0.0	1802.5 [375], 1735.4 [1211], 689.3 [4], 608.0 [3], 567.6 [3], ···91.2 [1]
	$^3B_1$ (C_{2v})	+93	2.0000	RuN: 1.819 NO: 1.182 ∠RuNO: 166.7 ∠NRuN: 130.7 ϕ(ONRuN): 0.0	/
NRuO−NO	^1A (C_1)	+182	/	RuO_t: 1.773 RuN_t: 1.660 RuN: 1.887 NO: 1.171 N_tRuO_t: 124.0 N_tRuN: 119.1 O_tRuN: 115.6 RuNO: 140.6 ϕ($ONRuO_t$: 143.7	1763.2 [751], 1044. [70], 822.8 [104], 557.1 [3], 388.8 [1], ···88.3 [28]
	^3A (C_1)	+195	2.0000	RuO_t: 1.775 RuN_t: 1.670 RuN: 1.895 NO: 1.175 N_tRuO_t: 118.5 N_tRuN: 109.4 O_tRuN: 119.0 ϕ($ONRuO_t$): −115.8	1774.7 [629], 1003.1 [52], 784.8 [83], 474.2 [3], 393.1 [2], ···86.7 [5]
$Ru(NO)_3$	^2A (C_3)	0	0.7502	RuN: 1.838 NO: 1.172 ∠RuNO: 164.0 ∠NRuN: 117.1	1803.2 [125], 1743.0 [1226], 556.3 [0], 527.7 [9], ···52.1 [3]
	$''^4A_2''$ (~D_{3h})	+109	3.7501	RuN: 1.871 NO: 1.179 ∠RuNO: 180.0 ∠NRuN: 120.0	/

ecules.[31] In these cases the bond lengths and angles presented in the tables are average values for these quantities.

$Ru(NO)_{1-3}$. RuNO and $Ru(NO)_2$ are the main products, analogous to the osmium system. Two bands almost obscured by the strong $(NO)_2$ absorption at 1790.8 and 1785.8 cm^{-1} in neon are appropriate for RuNO in different matrix sites (Figure 4), and examination of spectra from other metal nitrosyl systems confirms that these bands are unique to the ruthenium system. These bands grow in during annealing and are decreased on photolysis, though not to the same extent as was found for OsNO. No ^{15}N counterpart is observed because of masking by $(^{15}NO)_2$, but a band at 1712.3 cm^{-1} in the $^{15}N^{18}O$ experiment that exhibits the same annealing and photolysis behavior is appropriate for $Ru^{15}N^{18}O$. Both DFT functionals predict a $^2\Delta$

TABLE 8: Geometries, Energies, and Frequencies Calculated for Selected Neutral and Ionic Ruthenium Nitrosyls Using DFT (B3LYP/LanL2DZ/6-311+G(d))

molecule (ground state) [relative energy, kJ/mol]	$<S^2>$	geometry (Å, deg)	frequencies (cm^{-1}) [intensities (km/mol)]	ν(NO) scale factors	
				argon	neon
RuNO ($^2\Sigma^+$) [+50]	0.7501	RuN: 1.713 NO: 1.173 ∠NRuO: 180.0	1812.8 [693], 616.6 [2], 236.2 [22]	0.974	0.985
RuNO ($^2\Delta$) [0]	0.7574	RuN: 1.731 NO: 1.165 ∠NRuO: 180.0	1855.5 [722], 580.6 [5], 185.1 [34]×2	0.952	0.962
NRuO ($^2A''$) [+161]	0.8545	RuN: 1.652 RuO: 1.797 ∠NRuO: 118.5	1017.9 [55], 650.5 [23], 286.2 [10]	0.974 1.233	0.974 1.230
NRuO ($^2A'$) [+107]	0.7532	RuN: 1.639 RuO: 1.762 ∠NRuO: 125.4	1007.5 [20], 819.6 [130], 267.6 [9]	0.984 0.979	0.984 0.977
$RuNO^+$ ($^3\Delta$) [0]	2.0062	RuN: 1.801 NO: 1.129 ∠RuNO: 180.0	2030.4 [610], 514.6 [5], 257.1 [9]×2	/	/
$RuNO^+$ ($^1\Delta$) [+57]	0.1871	RuN: 1.784 NO: 1.128 ∠RuNO: 180.0	2033.2 [660], 551.2 [13], 225.3 [10]×2	/	/
$Ru(NO)_2$ ($^1A_1$)	/	RuN: 1.768 NO: 1.164 ∠RuNO: 154.9 ∠NRuN: 108.4	1870.4 [508], 1785.4 [1592], 713.5 [5], 623.5 [6], 585.2 [2], ⋯92.2 [1]	0.958	0.964
$Ru(NO)_3$ ($''^2A''$)	0.7634	RuN: 1.848 NO: 1.162 ∠RuNO: 154.3 ∠NRuN: 113.4	1879.8 [170], 1792.0 [1632]×2, 540.0 [0], 510.5 [12]x2, 464.2 [1], ⋯51.3 [3]	0.978	0.969

TABLE 9: Reaction Energies Calculated Using DFT

reaction	ΔE (BPW91) (kJ/mol)	ΔE (B3LYP) (kJ/mol)	reaction number
OsNO ($^2\Delta$) + NO ($^2\Pi$) → $Os(NO)_2$ ($^1A_1$)	−362	−285	1
$Os(NO)_2$ ($^1A_1$) + NO ($^2\Pi$) → $Os(NO)_3$ ($''^2A_1''$)	−184	−144	2
NOsO ($^2A''$) + NO ($^2\Pi$) → NOsO−NO ($^1A'$)	−216	/	3
RuNO ($^2\Delta$) + NO ($^2\Pi$) → $Ru(NO)_2$ ($^1A_1$)	−320	−232	4
$Ru(NO)_2$ ($^1A_1$) + NO ($^2\Pi$) → $Ru(NO)_3$ (^2A)	−139	−99	5
NRuO ($^2A'$) + NO ($^2\Pi$) → NRuO−NO (^1A)	−203	/	6

TABLE 10: Force Constants (Nm^{-1}) and Bond Angles (deg) Calculated for NOsO and NRuO Using Experimental Data

	f_{M-N}		f_{M-O}		$f_{M-N/M-O}$		bond angle	
metal	mean	std dev	mean	std dev	mean	std dev	mean	std dev
Os	849	3	710	3	79	21	111	22
Ru	711	10	547	10	110	34	115	20

TABLE 11: Comparison of Force Constants (Nm^{-1}) Calculated for NMN, OMO, and NMO (M = Os, Ru)

		Osmium		Ruthenium	
molecule	bond	f_{M-X}	$f_{M-X/M-Y}$	f_{M-X}	$f_{M-X/M-Y}$
NMN	M−N	722	115	588	115
NMO	M−N	849	79	711	110
	M−O	710		547	
OMO	M−O	828	72	694[a]	99[a]

[a] From ref 34.

ground state for RuNO, and the calculated frequencies support assignment of the observed bands to this species. Equivalent bands were observed in argon when dilute gas samples were used, within 17 cm^{-1} of the bands assigned to this molecule in neon. The $^{15}N^{16}O$ counterparts of the two sites are evident in the $^{14}N^{16}O$ + $^{15}N^{16}O$ argon matrix mixed isotopic experiment (Figure 5), though the $^{15}N^{18}O$ counterpart is partially obscured. The calculated $^{14}N^{16}O/^{15}N^{16}O$ and $^{15}N^{16}O/^{15}N^{18}O$ isotopic ratios of 1.0216 and 1.0220 are in good agreement with the experimental values of 1.0212 and 1.0214 (argon), confirming the assignment to RuNO. The $^{14}N^{16}O/^{15}N^{16}O$ ratio is relatively high but is lower than that in OsNO because the Ru−N bond is weaker and the coupling between the Ru−N and N−O modes is not as strong. The weaker bond is apparent in the lower calculated Ru−N stretching frequency of 625.2 cm^{-1} compared to 696.1 cm^{-1} calculated for OsNO despite the lower mass of ruthenium.

The nitrosyl stretching modes for $Ru(NO)_2$ are observed at 1805.3 and 1721.4 cm^{-1} in neon, but only the more intense antisymmetric mode is observed in argon at 1709.6 cm^{-1}. The mixed isotopic experiment in neon shows a clear triplet for the lower frequency band (Figure 4), but the yield of $Ru(NO)_2$ is lower and the 1805.3 cm^{-1} band and isotopic counterparts are not observed. As with $Os(NO)_2$, the DFT calculations predict a singlet ground state for $Ru(NO)_2$, with nitrosyl stretching frequencies in good agreement with experiment. The calculated isotopic ratios of 1.0202 and 1.0245 for the antisymmetric nitrosyl stretching mode are close to the experimental values of 1.0201 and 1.0236 (neon).

Bands at 1738.9 and 1731.6 cm^{-1} in argon are appropriate for the degenerate stretching mode of $Ru(NO)_3$ in different matrix sites, again analogous to both the iron and osmium nitrosyl systems. The DFT calculations for $Ru(NO)_3$ predict a singlet ground state, with frequencies that are compatible with these observed bands, and calculated isotopic ratios of 1.0194 and 1.0256 are in good agreement with experimental values of 1.0196 and 1.0243. However, the spectra are too congested to see any intermediate components in the mixed isotopic experi-

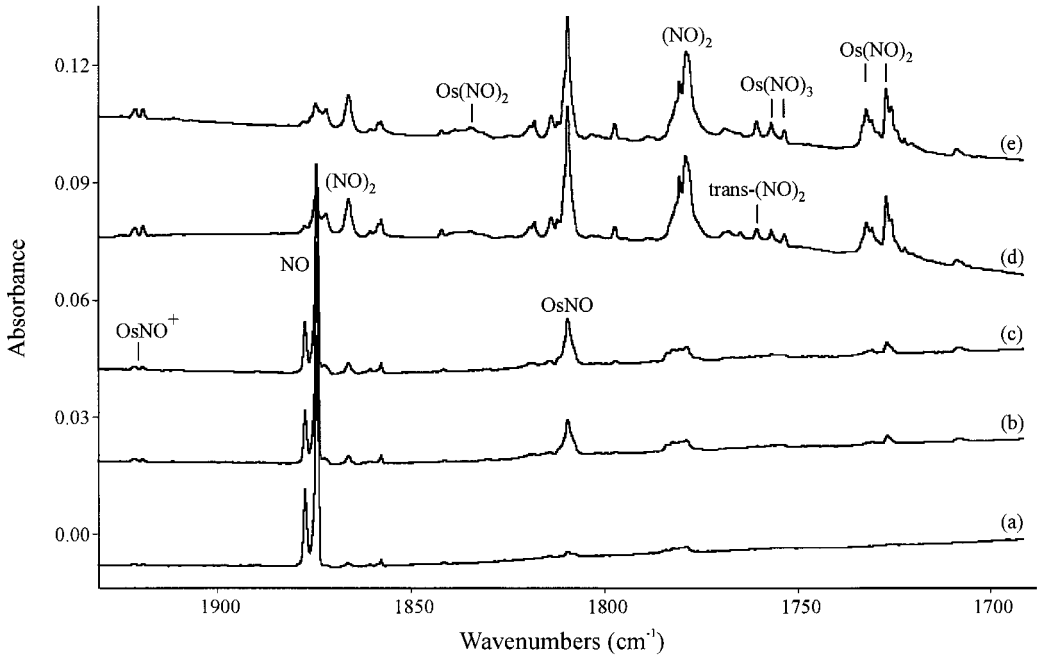

Figure 1. Infrared spectra in the 1930−1690 cm^{-1} region for samples prepared by co-condensation of laser-ablated osmium atoms: (a) after 25 min deposition with 0.04% NO in neon, (b) after annealing to 7 K, (c) after annealing to 9 K, (d) after annealing to 11 K, (e) after annealing to 12 K.

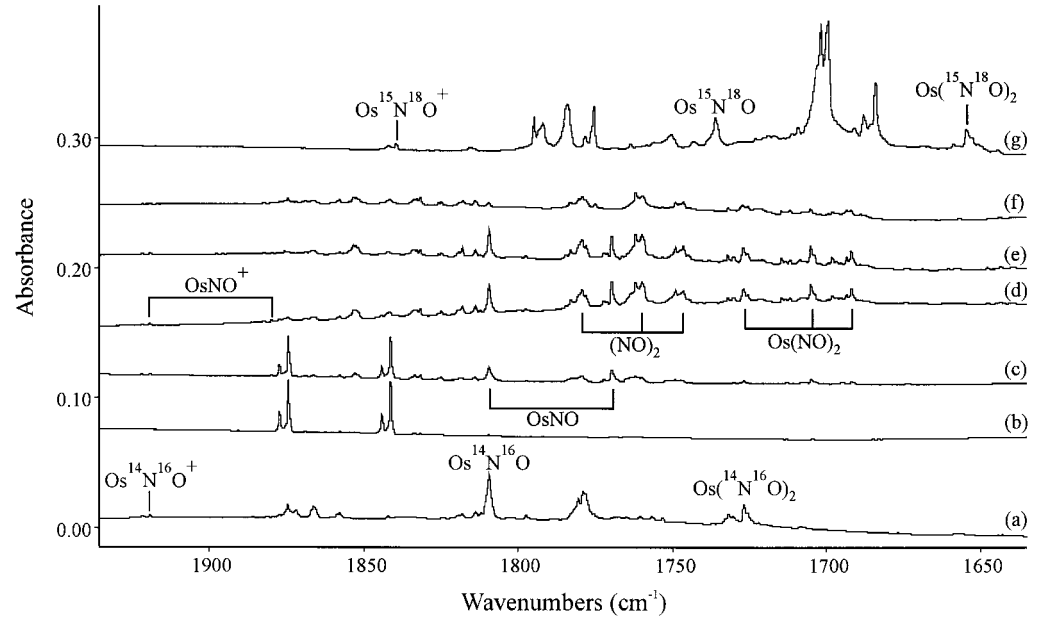

Figure 2. Infrared spectra in the 1930−1680 cm^{-1} region for samples prepared by co-condensation of laser-ablated osmium atoms: (a) after 25 min deposition with 0.04% NO in neon and annealing to 11 K, (b) after 30 min deposition with 0.02% NO + 0.02% ^{15}NO in neon, (c) after annealing to 9 K, (d) after annealing to 11 K, (e) after annealing to 12 K, (f) after 20 min photolysis, and (g) after 50 min deposition with 0.11% $^{15}N^{18}O$ in neon and annealing to 10 K.

ments that would confirm this assignment. Weak bands observed in neon near 1750 cm^{-1} with very similar ratios are most likely due to $Ru(NO)_3$.

The calculated energies of the addition reactions that form the $M(NO)_{2,3}$ complexes are listed in Table 9. All are strongly exothermic, though the energy release is considerably greater for the formation of the dinitrosyl complexes. The greater exothermicity in the reactions of the osmium nitrosyls compared to ruthenium is consistent with the stronger metal−ligand bonding expected for osmium, as discussed below.

In summary, the osmium and ruthenium complexes are modeled well with DFT and have the same ground states and geometries observed for $Fe(NO)_{1-3}$.[7]

NOsO and NRuO. Weak bands are observed on deposition of osmium and NO in neon at 1057.6 and 890.5 cm^{-1} that grow in during annealing and greatly increase on photolysis. Figure 6 shows the spectrum for the $^{14}NO+^{15}NO$ sample and contrasts the spectra from other isotopic experiments. Similar bands are observed in argon at 1052.0 and 886.9 cm^{-1} and exhibit the same behavior. These frequencies are too low for nitrosyl stretching modes, but are appropriate for Os−N and Os−O vibrations. The upper band shows a large ^{15}N shift but is unaffected on ^{18}O substitution. The lower band shows the opposite behavior, and the mixed isotopic experiments reveal isotopic doublets and confirm that only one nitrogen and one oxygen atom are involved. The above findings support the

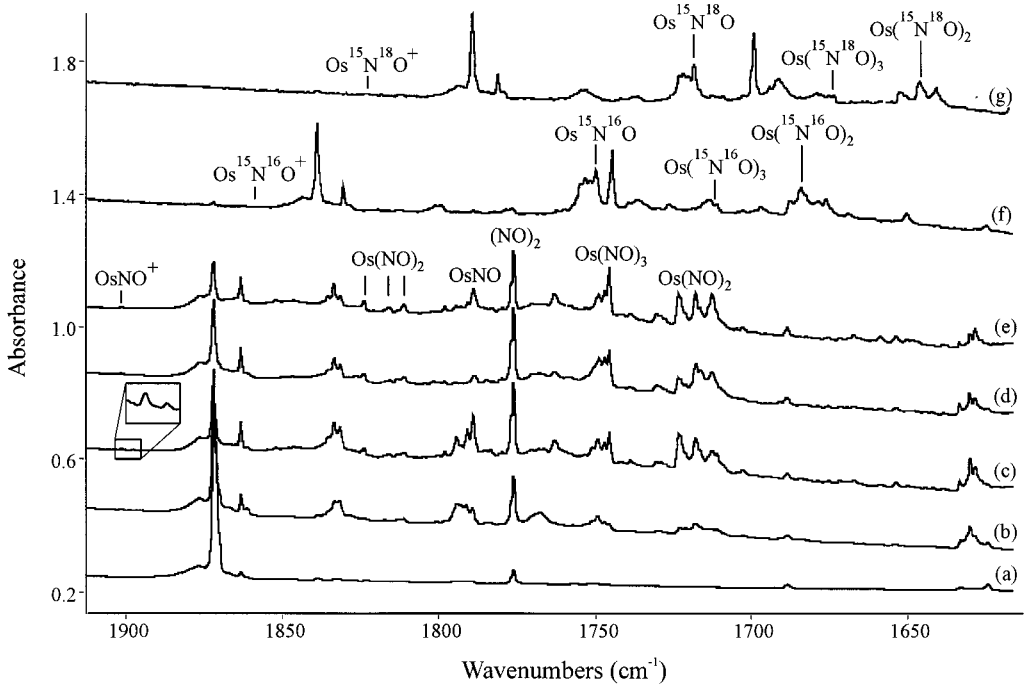

Figure 3. Infrared spectra in the 1910−1620 cm^{-1} region for samples prepared by co-condensation of laser-ablated osmium atoms: (a) after 85 min deposition with 0.3% NO in argon, (b) after annealing to 25 K, (c) after annealing to 40 K, (d) after 25 min photolysis, (e) after annealing to 45 K, (f) after deposition with 0.3% ^{15}NO in argon and annealing to 30 K, (g) after deposition with 0.3% $^{15}N^{18}O$ in argon and annealing to 30 K.

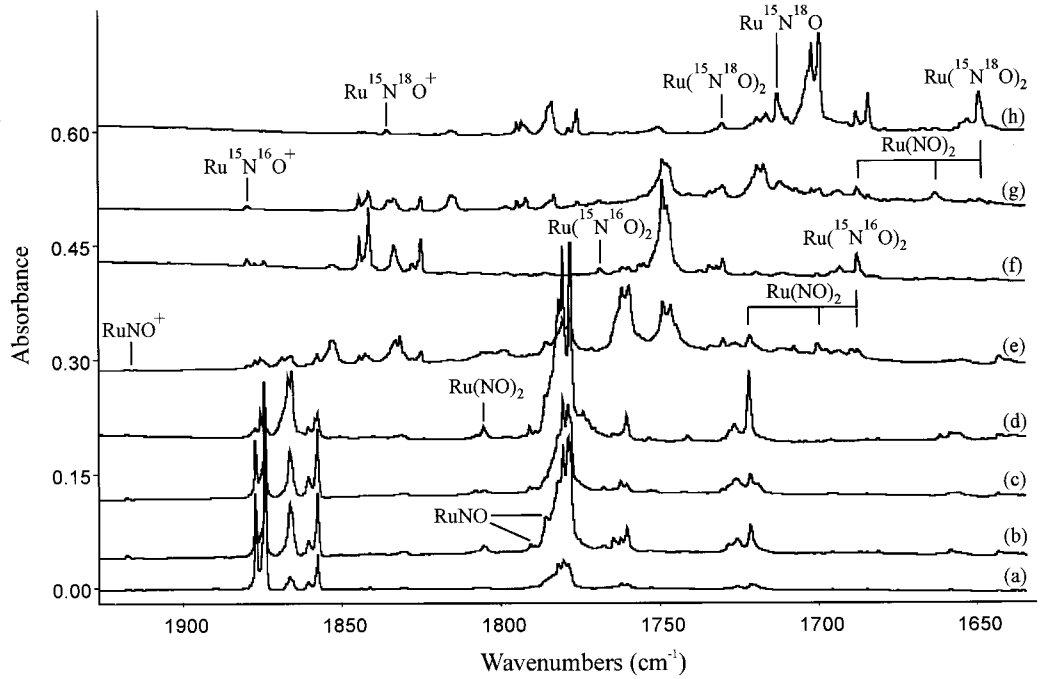

Figure 4. Infrared spectra in the 1920−1640 cm^{-1} region for samples prepared by co-condensation of laser-ablated ruthenium atoms: (a) after 55 min deposition with 0.14% NO in neon, (b) after annealing to 9 K, (c) after 15 min photolysis, (d) after annealing to 12 K, (e) after deposition with 0.11% NO and 0.11% ^{15}NO in neon and annealing to 10 K, (f) after deposition with 0.1% ^{15}NO in neon and annealing to 10 K, (g) after deposition with 0.1% ^{15}NO and 0.07% $^{15}N^{18}O$ in neon and annealing to 9 K, (h) after deposition with 0.11% $^{15}N^{18}O$ in neon and annealing to 11 K.

assignment of these bands to the insertion product NOsO, which has precedent in most of the metal nitrosyl studies performed in this laboratory.[7−16] The isotopic data shows that the Os−N and Os−O vibrations are largely uncoupled, and the $^{14}N^{16}O/^{15}N^{16}O$ and $^{15}N^{16}O/^{15}N^{18}O$ isotopic ratios of 1.0305 and 1.0517 are close to harmonic Os−N and Os−O diatomic ratios of 1.0326 and 1.0555. The substantial growth on annealing suggests that osmium atoms can insert into the N−O bond, as was found with osmium and dinitrogen.[29] The combination of OsN and OsO with oxygen and nitrogen atoms alone is not sufficient to account for the increase of these bands, since strong growth is observed in experiments with concentrations of only 0.02% NO/Ne, when absorptions due to OsN are not observable after deposition,[29] though such additions are also occurring, as shown by the growth of bands due to NOsN and OOsO. The strong growth on photolysis and the corresponding decrease of OsNO indicate that the mononitrosyl is almost completely converted to NOsO on photolysis. The fact that both OsNO and NOsO increase during annealing suggests that the relative orientation of the reactants determines which product is formed when the

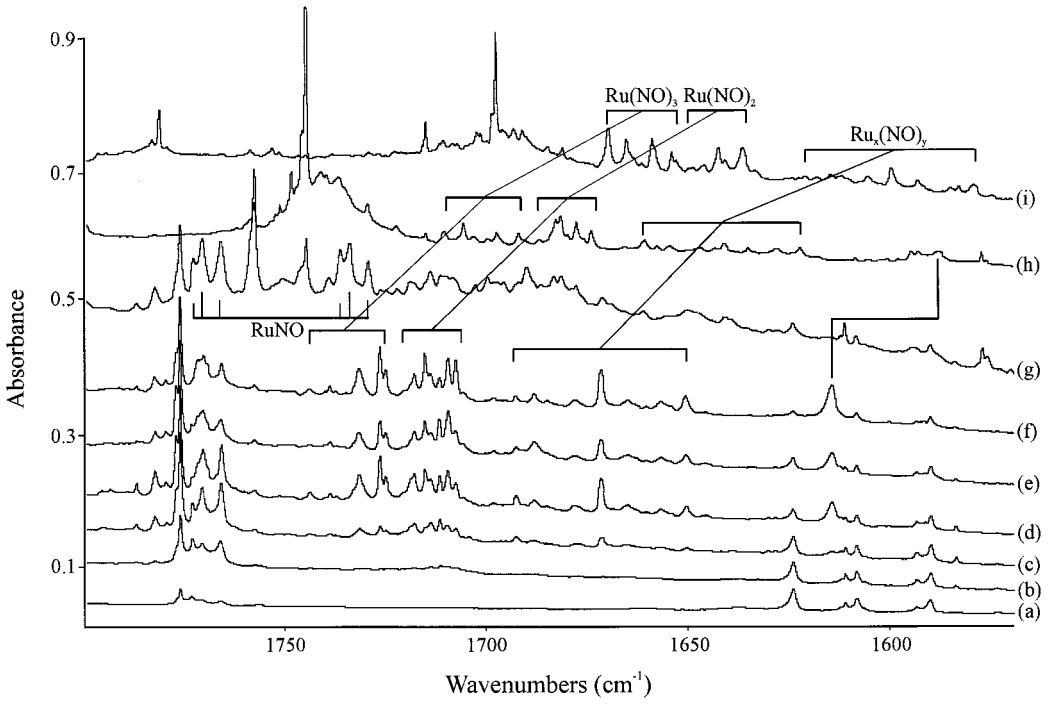

Figure 5. Infrared spectra in the 1800−1560 cm^{-1} region for samples prepared by co-condensation of laser-ablated ruthenium atoms: (a) after 55 min deposition with 0.1% NO in argon, (b) after annealing to 25 K, (c) after annealing to 30 K, (d) after annealing to 40 K, (e) after 23 min photolysis, (f) after annealing to 45 K, (g) after deposition with 0.25% NO and 0.25% ^{15}NO in argon at 30 K, (h) after deposition with 0.3% ^{15}NO in argon and annealing to 40 K, (i) after deposition with 0.3% $^{15}N^{18}O$ in argon and annealing to 40 K.

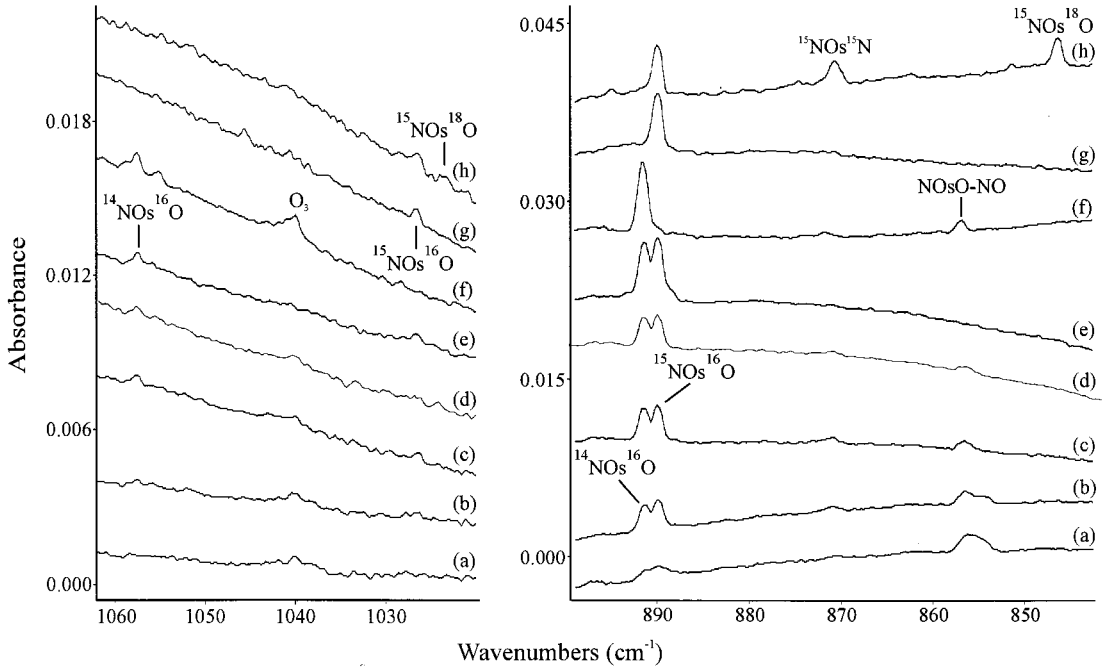

Figure 6. Infrared spectra in the 1060−1020 and 890−840 cm^{-1} regions for samples prepared by co-condensation of laser-ablated osmium atoms: (a) after 30 min deposition with 0.02% NO and 0.02% ^{15}NO in neon, (b) after annealing to 9 K, (c) after annealing to 11 K, (d) after annealing to 12 K, (e) after 20 min photolysis, (f) after 25 min deposition with 0.04% NO in neon and annealing to 11 K, (g) after 25 min deposition with 0.12% ^{15}NO in neon and annealing to 10 K, (h) after 45 min deposition with 0.1% ^{15}NO and 0.07% $^{15}N^{18}O$ in neon and annealing to 12 K.

reactants encounter each other, and that a sufficiently large barrier exists between them that interconversion between the structural isomers is not possible until the sample is irradiated with UV/visible light. Clearly the reactions are under kinetic and not thermodynamic control.

The ruthenium analogue, NRuO, is also observed with bands at 991.5 and 800.4 cm^{-1} that grow significantly on photolysis but do not show any growth on annealing (Figure 7). The respective nitrogen and oxygen isotopic ratios of 1.0291 and 1.0482 for these bands are slightly less than pure Ru−N and Ru−O harmonic ratios of 1.0306 and 1.0517, which shows very little mixing between the two modes.

DFT calculations for these species predict doublet ground states with bent geometries, and the calculated frequencies and relative intensities are in good agreement with experiment, though not as good as for the metal nitrosyls. The poorer agreement with experiment for DFT calculations of NMO species has been found with other transition metals. The

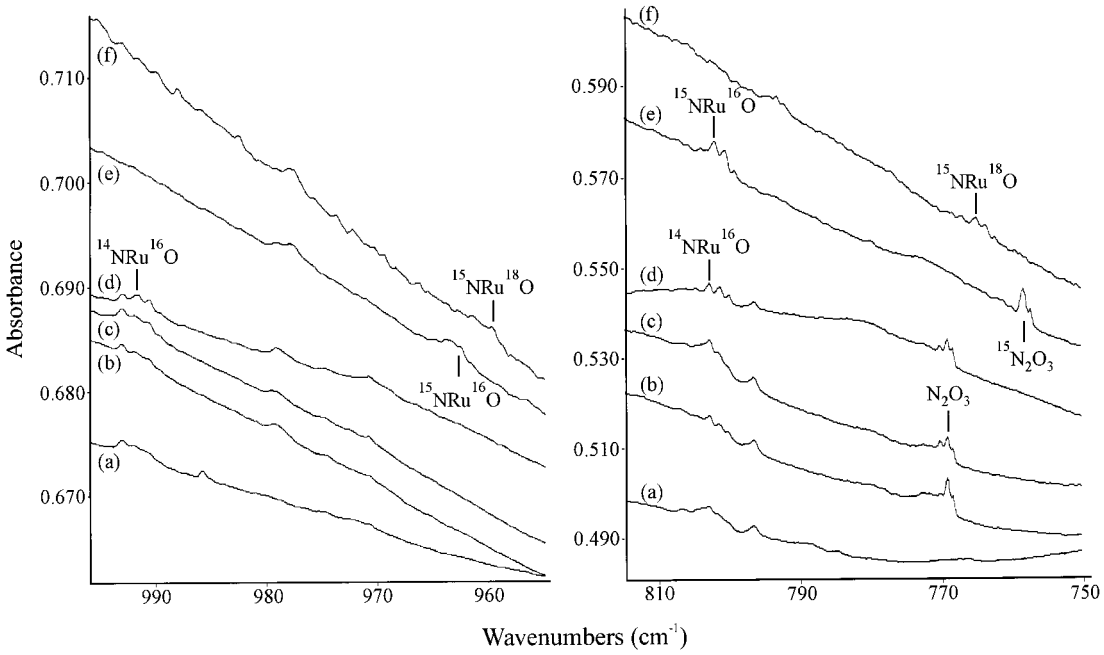

Figure 7. Infrared spectra in the 995−955 and 810−760 cm^{-1} regions for samples prepared by co-condensation of laser-ablated ruthenium atoms: (a) after 60 min deposition with 0.3% NO and argon, (b) after annealing to 30 K, (c) after 30 min photolysis, (d) after annealing to 35 K, (e) after 60 min deposition with 0.3% ^{15}NO in argon and annealing to 35 K, (f) after 60 min deposition with 0.3% $^{15}N^{18}O$ in argon and annealing to 35 K.

experimental data presented for the various NMO molecules isolated in this laboratory provides a means by which the effectiveness of different theoretical treatments can be assessed. In the case of NOsO, the $^2A''$ state is calculated lower than the $^2A'$ state by 72 and 67 kJ/mol using the BPW91 and B3LYP functionals respectively, and the former is identified as the ground state. In both cases the quartet states are higher in energy and do not have frequencies compatible with experiment. In previous DFT calculations for other NMO molecules, the BP86 functional, which is found to give similar results to the BPW91 functional, invariably overestimates the M−N stretching frequency to a greater extent than is found for the N−O stretching mode of the MNO molecule, of the order of 50−60 cm^{-1}.[8−16] This is the case for the $^2A''$ state which has an Os−N frequency 52 cm^{-1} higher than the neon value. The Os−O frequency calculated for the $^2A''$ state is in very good agreement with experiment, also in line with previous results for this class of molecule. The results are less clear for NRuO, where the $^2A''$ state is calculated to be 12 kJ/mol *lower* than the $^2A'$ state using the BPW91 functional but 54 kJ/mol *higher* with the B3LYP functional. The BPW91 calculated frequencies for the two states are very similar, but the B3LYP frequencies for the $^2A''$ state are anomalous, and indicate that $^2A'$ is the correct ground state for NRuO. The calculated isotopic ratios for both molecules show the expected lack of coupling between the M−N and M−O stretching modes, the respective $^{14}N^{16}O/^{15}N^{16}O$ and $^{15}N^{16}O/^{15}N^{18}O$ ratios of 1.0312 and 1.0536 for NOsO and 1.0305 and 1.0510 for NRuO being in good agreement with experiment.

Os[NO]. The existence of metastable states of the OsNO and RuNO fragments and their sensitivity to light is consistent with the behavior of the M−NO group in the $Na_2[M(CN)_5NO]$ complexes (M = Fe, Ru, Os).[1−6] Available X-ray diffraction and infrared data for these compounds indicate that the binding of the nitrosyl group to the metal is altered to the oxygen-bound and side-bound forms in the excited states. These arrangements are predicted to be only weakly stable in the isolated [Fe,N,O] system,[32] but the side-bound Fe[NO] molecule Fe-η^2-NO is observed with absorptions at 1343.8 and 1342.2 cm^{-1} in argon and neon, respectively. Apparently interactions with the host matrix stabilize the side-bound geometry, but not FeON, for which there is no experimental evidence.[7]

The side-bound and oxygen-bound structures of OsNO and RuNO have been calculated in different electronic states, and are found to be considerably higher in energy than the M-η^1-NO mononitrosyls and the NMO insertion products. These metastable structures are probably not observable in the gas phase, where they would rapidly convert to a more stable form, but they can, in principle, be trapped in an inert matrix at low temperature. Both the BPW91 and B3LYP functionals predict a stable cyclic Os[NO] molecule in a $^2A'$ state, the $^2A''$ state opens during geometry optimization, and the quartet state is much higher in energy (Tables 5 and 6). The $^2A'$ state Os[NO] molecule is 68 kJ/mol (B3LYP) and 159 kJ/mol (BPW91) more stable than Os and NO so this product might also be trapped in the matrix. The N−O stretching frequencies computed for Os[NO] are 1202.2 and 1268.1 cm^{-1}, using the BPW91 and B3LYP functionals, respectively. Close examination of the osmium/argon spectra reveals weak bands at 1154.5 and 1149.5 cm^{-1} that are not present after deposition but appear during annealing. The isotopic counterparts exhibit $^{14}N^{16}O/^{15}N^{16}O$ and $^{15}N^{16}O/^{15}N^{18}O$ ratios of 1.0182 and 1.0258, close to the ratios of 1.0179 and 1.0277 observed for free nitric oxide in argon. This is in contrast to the ratios observed for OsNO, where the nitrogen isotopic ratio is much higher. The isotopic ratios calculated for Os[NO] using the BPW91 functional are 1.0190 and 1.0263, in good agreement with those for the observed bands. These comparisons support assignment of the 1154.5 and 1149.5 cm^{-1} bands to the side-bound Os[NO] in different matrix sites. However, these bands are insensitive to photolysis, which is surprising considering the strong response of OsNO and NOsO to light. Another band observed in argon that grows in during annealing at 1132.6 cm^{-1} is completely destroyed on photolysis, but has isotopic ratios of 1.0165 and 1.0283, quite different to the values calculated by DFT. This is probably the correct assignment, but the high lying weakly bound metastable geometries are harder to model with DFT, which can only give approximate results.

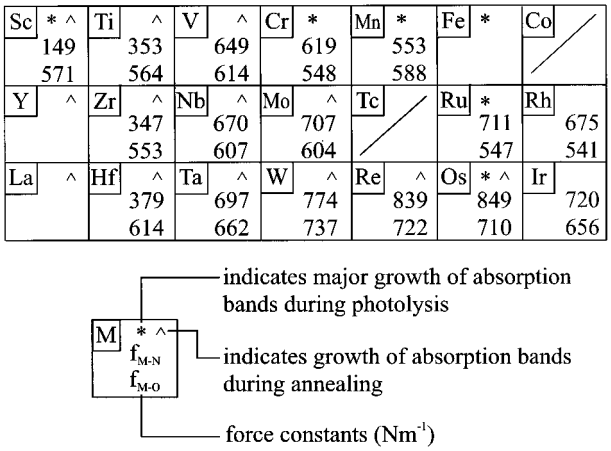

Figure 8. Summary of force constants calculated for matrix isolated NMO molecules (M = transition metal).

The calculations for Ru[NO] predict a $^2A''$ state, and other doublet and quartet states have open structures. The N−O stretching frequency for this state is calculated at 1255.7 and 1392.2 cm^{-1} using the BPW91 and B3LYP functionals, respectively. However, no bands unique to the ruthenium system are observed in this region, and no assignment to Ru[NO] can be made.

Calculations on both OsON and RuON were also performed, and the results are included in the data tables, but no likely candidate bands were observed that could be assigned to these isomers.

Bonding in NMO Molecules. The most important difference between the two metals is the relative stabilities of the insertion product NMO and the end-bonded mononitrosyl complex MNO as calculated by DFT; the insertion product is lower for osmium and the linear nitrosyl complex is preferred for ruthenium. The barrier between these structures is large enough to prevent their interconversion at low temperature in the matrix, but during photolysis all OsNO rearranges to the more stable NOsO form. In like fashion RuNO is isomerized to NRuO on photolysis even though it is the less stable geometry since excited molecules that rearrange to the metastable NRuO geometry are unable to rearrange back to RuNO when their excess energy is subsequently relaxed by the matrix cage. However, NRuO is not formed on annealing, which indicates that the insertion reaction is an activated process.

This fundamental difference between the Os and Ru metals is explained by the much stronger bonds in NOsO relative to NRuO, as shown by the experimentally derived force constants in Table 10. These were calculated by neglecting the bending mode, for which no data is available, and solving for the M−N and M−O force constants, the sretch−stretch interaction constant, and the bond angle. Eleven different sets of values for these parameters were derived using all available isotopic data. The stretching force constants show little uncertainty and represent good estimates for these quantities within the model used. The other parameters show considerable uncertainty, but indicate that both NOsO and NRuO are nonlinear and have positive sretch−stretch interaction force constants. The same calculations have been performed for the other NMO molecules observed in this laboratory,[8−16] and the derived force constants are shown in Figure 8. The uncertainties in these values are similar to those found for NRuO and NOsO, and only the stretching force constants are given. All molecules are found to be bent, but there is some variability in the sign of the interaction constant. This quantity is positive for all second and third row transition metals except hafnium, for which the uncertainty is too large to determine the sign. The titanium interaction force constant has a negative value, but values for the other first row transition metals are too small and uncertain to determine their sign. The NMO molecules that increase on annealing in a spontaneous reaction without activation energy and on photochemical excitation are indicated in Figure 8. It is clear that the third row transition metals have the strongest bonds, and all show an increase of NMO during annealing beyond that expected for simple atom addition reactions to MO or MN species. The first row metals have the weakest bonds: the early metals Sc, Ti, and V insert spontaneously on annealing in the cold matrix, the middle metals Cr, Mn, and Fe require photochemical excitation, and the later metals Co, Ni, and Cu do not insert at all.[7−15] (The growth of NScO on photolysis may be due to isomerization of Sc[NO]).[10] Titanium is the most reactive: NTiO grows strongly on annealing but decreases slightly on photolysis.[10] The NMO molecules of the second row transition metals show a mixture of these traits. It is noteworthy that no such species were identified for the Group 10 and 11 metals, probably because more antibonding orbitals are occupied in the later transition metals. There is insufficient data available to calculate the force constants in NFeO, as only one mixed stretching mode was observed.[7] However, a detailed theoretical study of the [Fe,N,O] isomers showed the insertion product to be 100 kJ/mol higher in energy than the linear FeNO molecule,[32] which suggests that the bonds are considerably weaker than those in NRuO.

It is also useful to compare the force constants in NOsO and NRuO with those in the dioxides and dinitrides of these metals,[29,33,34] which are shown in Table 11. The M−N bond in NMO is much stronger than in NMN, and the M−O bond is weakened by a comparable amount relative to OMO. This can be explained by the smaller energy difference between the metal and nitrogen valence orbitals, strengthening the interaction between these atoms at the expense of the metal−oxygen bond.

NOsO−NO. A weak band is observed in osmium experiments at 857.2 cm^{-1} on deposition in neon (Figure 6), with corresponding $^{15}N^{16}O$ and $^{15}N^{18}O$ bands at 856.5 and 814.0 cm^{-1}. These bands decrease on annealing and on photolysis. The argon $^{14}N^{16}O$ and $^{15}N^{18}O$ counterparts are at 850.0 and 806.0 cm^{-1}, the $^{15}N^{16}O$ band was not observed. The oxygen isotopic ratio of 1.0522 and negligible nitrogen shift are very similar to those observed for NOsO, and the bands are clearly due to a species derived from this molecule. Two possibilities are considered using DFT, the nitrosyl complex NOsO−NO and OOsNO, perhaps derived from insertion by the metal into NO_2 during deposition. The OOsNO molecule is nonlinear with a doublet ground state (not included in Table 5), the quartet state being 30 kJ/mol higher in energy. The Os−O stretching mode is calculated to be 939.9 cm^{-1}, higher than the observed mode, with a $^{15}N^{16}O/^{15}N^{18}O$ ratio of 1.0557, in poor agreement with experiment. The same mode has a frequency of 872.3 cm^{-1} in the quartet calculation, close to the observed value, but the isotopic ratio of 1.0559 is still incorrect. The calculations for the complexed NOsO molecule are more encouraging. The $^1A'$ state has the lowest energy and has a largely uncoupled Os−O mode with frequency 916.2 cm^{-1} and $^{15}N^{16}O/^{15}N^{18}O$ ratio of 1.0529, in reasonable agreement with experiment. The ^3A state is only 4 kJ/mol higher, and has a similar mode with frequency 887.1 cm^{-1} and ratio 1.0533, in better agreement with experiment than the singlet state. The $^1A''$ state was also calculated, but was over 180 kJ/mol higher in energy and is not included in Table 5. The nitrosyl stretching modes for these states, 1842.0

and 1763.9 cm^{-1} respectively, should be observable, but no suitable bands were observed in the nitrosyl stretching region, perhaps obscured by other bands. The observed bands are therefore tentatively assigned to NOsO−NO, probably in the triplet state. No such bands were observed for ruthenium, though DFT predicts that the addition reaction is exothermic (Table 9).

$OsNO^+$ and $RuNO^+$. The $OsNO^+$ ion is observed in both neon and argon experiments as a weak doublet of matrix sites. No intermediate is observed in mixed isotopic experiments, confirming that only one nitrosyl group is involved. Both DFT functionals predict two triplet states, $^3\Sigma^-$ and $^3\Delta$, almost identical in energy, with the singlet states somewhat higher. The predicted frequencies are quite different, however, and the values 1956.6 and 2011.5 cm^{-1} calculated for the $^3\Delta$ state using the BPW91 and B3LYP functionals are in good agreement with experiment, using the results for OsNO and $Os(NO)_2$ as a guide. The frequencies for the $^3\Sigma^-$ state are too high, and therefore $^3\Delta$ is identified as the ground state for $OsNO^+$. The isotopic frequency ratios 1.0215 and 1.0223 calculated for this state are in good agreement with the experimental values of 1.0209 and 1.0219 (Table 1). The $OsNO^+$ absorption is greatly enhanced relative to the OsNO band when the reagent gas is doped with the electron trap CCl_4, lending more support to this assignment.[7]

The $RuNO^+$ ion is also predicted to have a $^3\Delta$ ground state with both functionals, with the BPW91 nitrosyl stretching frequency only slightly higher than a weak band observed at 1918.0 cm^{-1} in neon that grows during annealing but decreases on photolysis. The $^{15}N^{16}O$ and $^{15}N^{18}O$ counterparts are observed at 1879.7 and 1835.6 cm^{-1}, giving isotopic ratios of 1.0205 and 1.0240, respectively. The DFT calculated ratios of 1.0200 and 1.0249 are consistent with this result and support assignment of the 1918.0 cm^{-1} band to $RuNO^+$ in solid neon. No such band is observed in argon, even when CCl_4 is used.

The corresponding anion complexes $OsNO^-$ and $RuNO^-$ are not observed, either because they were not formed or because they were obscured by other bands.

$Ru_x(NO)_y$. Additional bands are observed in argon in the range 1693−1650 cm^{-1} that grow in during annealing when the concentration of ruthenium atoms is increased. The isotopic counterparts are observed in experiments using $^{15}N^{16}O$ and $^{15}N^{18}O$, but the mixed isotopic experiments are too congested to distinguish any multiplet structures. These bands are very similar in frequency and overall appearance to the bands due to $Pd_x(NO)_y$ cluster species previously observed in this laboratory[16] and are probably due to ruthenium cluster species. The equivalent osmium cluster species were not observed as no experiments were performed with sufficiently high concentrations of osmium atoms.

Conclusions

Laser-ablated osmium and ruthenium atoms react with nitric oxide to form the complexes $Os(NO)_{1-3}$ and $Ru(NO)_{1-3}$ and the insertion products NOsO and NRuO. With the exception of NRuO, those products increase during annealing which indicates that no kinetic or electronic excitation is required for these reactions to occur. DFT calculations accurately model these species and provide frequencies and corresponding isotopic frequency ratios of chemically significant accuracy. Unlike iron and ruthenium, the osmium insertion product NOsO is found to be more stable than the mononitrosyl complex OsNO, and this is attributed to the high Os−N and Os−O bond strengths in this molecule, as indicated by the frequencies and derived force constants. Both OsNO and NOsO coexist in neon and argon matrices, but virtually all OsNO is converted to the more stable NOsO isomer on exposure to UV/visible light. This behavior mirrors that for osmium nitrosyl complexes in solid-state materials, which exhibit long-lived metastable states and sensitivity to light irradiation.[1−6]

Acknowledgment. We thank N.S.F. and P.R.F. for financial support and M.F. Zhou for assistance with several Ru experiments.

References and Notes

(1) Carducci, M. D.; Pressprich, M. R.; Coppens, P. *J. Am. Chem. Soc.* **1997**, *119*, 2669.

(2) Guida, J. A.; Piro, O. E.; Aymonino, P. J. *Inorg. Chem.* **1995**, *34*, 4113.

(3) Guida, J. A.; Aymonino, P. J.; Piro, O. E.; Castellano, E. E. *Spectrochim. Acta*, **1993**, *49A*, 535.

(4) Woike, Th.; Haussuhl, S. *Solid State Commun.* **1993**, *86*, 333.

(5) Woike, Th.; Zollner, H.; Krasser, W.; Haussuhl, S. *Solid State Commun.* **1990**, *73*, 149.

(6) Guida, J. A.; Piro, O. E.; Aymonino, P. J. *Solid State Commun.* **1986**, *57*, 175.

(7) Zhou, M. F.; Andrews, L. *J. Phys. Chem. A* **2000**, *104*, 3915 (Fe + NO) and references therein.

(8) Andrews, L.; Zhou, M. F.; Ball, D. W. *J. Phys. Chem. A* **1998**, *102*, 10041 (Mn, Re + NO).

(9) Zhou, M. F.; Andrews, L. *J. Phys. Chem. A* **1998**, 102, 10025 (Nb, Ta + NO).

(10) Kushto, G.; Zhou, M. F.; Andrews, L. *J. Phys. Chem. A* **1999**, 103, 1115 (Ti, Sc + NO).

(11) Kushto, G.; Andrews, L. *J. Phys. Chem. A* **1999**, 103, 4836 (Ti, Zr, Hf + NO).

(12) Zhou, M. F.; Andrews, L. *J. Phys. Chem. A* **1999**, 103, 478 (V + NO).

(13) Zhou, M. F.; Andrews, L. *J. Phys. Chem. A* **1998**, 102, 7452 (Cr + NO).

(14) Andrews, L.; Zhou, M. F. *J. Phys. Chem. A* **1999**, 103, 4167 (Mo, W + NO).

(15) Zhou, M. F.; Andrews, L. *J. Phys. Chem. A* **2000**, *104*, 2618 (Cu + NO).

(16) Citra, A.; Andrews, L. *J. Phys. Chem. A* **2000**, *104*, 8160. (Pt, Pd + NO).

(17) Chen, Y.; Lin, F. T.; Shepherd, R. E. *Inorg. Chem.* **1999**, *38*, 973.

(18) Burkholder, T. R.; Andrews, L. *J. Chem. Phys.* **1991**, *95*, 8697.

(19) Bare, W. D.; Citra, A.; Chertihin, G. V.; Andrews, L. *J. Phys. Chem. A* **1999**, *103*, 5456.

(20) Frisch, M. J.; Trucks, G. W.; Schlegel, H. B.; Gill, P. M. W.; Johnson, B. G.; Robb, M. A.; Cheeseman, J. R.; Keith, T.; Petersson, G. A.; Montgomery, J. A.; Raghavachari, K.; Al-Laham, M. A.; Zakrzewski, V. G.; Ortiz, J. V.; Foresman, J. B.; Cioslowski, J.; Stefanov, B. B.; Nanayakkara, A.; Challacombe, M.; Peng, C. Y.; Ayala, P. Y.; Chen, W.; Wong, M. W.; Andres, J. L.; Replogle, E. S.; Gomperts, R.; Martin, R. L.; Fox, D. J.; Binkley, J. S.; Defrees, D. J.; Baker, J.; Stewart, J. P.; Head-Gordon, M.; Gonzalez, C.; Pople, J. A. *Gaussian 94, Revision B.1*; Gaussian, Inc.: Pittsburgh, PA, 1995.

(21) Becke, A. D. *Phys. Rev. A* **1988**, *38*, 3098.

(22) Perdew, J. P.; Wang, Y. *Phys. Rev. B* **1992**, *45*, 13244.

(23) Becke, A. D. *J. Chem. Phys.* **1993**, *98*, 5648.

(24) Krishnan, R.; Binkley, J. S.; Seeger, R.; Pople, J. A. *J. Chem. Phys.* **1980**, *72*, 650.

(25) Wadt, W. R.; Hay, P. J. *J. Chem. Phys.* **1985**, *82*, 284.

(26) Hay, P. J.; Wadt, W. R. *J. Chem. Phys.* **1985**, *82*, 299.

(27) Jacox, M. E. *Chem. Phys.* **1994**, *189*, 149.

(28) Bytheway, I.; Wong, M. W.; *Chem. Phys. Lett.* **1998**, *282*, 219.

(29) Citra, A.; Andrews, L. *J. Phys. Chem. A* **2000**, *104*, 1152.

(30) Adams, D. M. *Metal−Ligand and Related Vibrations*; Edward Arnold (Publishers) Ltd.: London, 1967.

(31) Sherrill, C. D.; Lee, M. S.; Head-Gordon, M. *Chem. Phys. Lett.* **1999**, *302*, 425.

(32) Fiedler, A.; Iwata, S. *J. Phys. Chem. A* **1998**, *102*, 3618.

(33) Zhou, M.; Citra, A.; Liang, B.; Andrews, L. *J. Phys. Chem. A* **2000**, *104*, 3457 (Ru, $Os+O_2$).

(34) Kay, J. G.; Green, D. W.; Duca, K.; Zimmerman, G. L. *J. Mol. Spectrosc.* **1989**, *138*, 49.